Cell Reports
Article

Disruption of *Runx1* and *Runx3* Leads to Bone Marrow Failure and Leukemia Predisposition due to Transcriptional and DNA Repair Defects

Chelsia Qiuxia Wang,[1,2,5] Vaidehi Krishnan,[1,5] Lavina Sierra Tay,[1,5] Desmond Wai Loon Chin,[1] Cai Ping Koh,[1] Jing Yuan Chooi,[1] Giselle Sek Suan Nah,[1,2] Linsen Du,[1] Bindya Jacob,[1] Namiko Yamashita,[1] Soak Kuan Lai,[1] Tuan Zea Tan,[1] Seiichi Mori,[1] Ichiro Tanuichi,[3] Vinay Tergaonkar,[2,*] Yoshiaki Ito,[1,2,*] and Motomi Osato[1,2,4,*]
[1]Cancer Science Institute of Singapore, National University of Singapore, Singapore 117599, Singapore
[2]Institute of Molecular and Cell Biology, A*STAR, Singapore 138673, Singapore
[3]Laboratory for Transcriptional Regulation, RIKEN Center for Integrative Medical Sciences, Yokohama, Kanagawa 230-0045, Japan
[4]Institute of Bioengineering and Nanotechnology, A*STAR, Singapore 138669, Singapore
[5]Co-first author
*Correspondence: vinayt@imcb.a-star.edu.sg (V.T.), csiitoy@nus.edu.sg (Y.I.), csimo@nus.edu.sg (M.O.)
http://dx.doi.org/10.1016/j.celrep.2014.06.046

SUMMARY

The RUNX genes encode transcription factors involved in development and human disease. *RUNX1* and *RUNX3* are frequently associated with leukemias, yet the basis for their involvement in leukemogenesis is not fully understood. Here, we show that *Runx1;Runx3* double-knockout (DKO) mice exhibited lethal phenotypes due to bone marrow failure and myeloproliferative disorder. These contradictory clinical manifestations are reminiscent of human inherited bone marrow failure syndromes such as Fanconi anemia (FA), caused by defective DNA repair. Indeed, *Runx1;Runx3* DKO cells showed mitomycin C hypersensitivity, due to impairment of monoubiquitinated-FANCD2 recruitment to DNA damage foci, although FANCD2 monoubiquitination in the FA pathway was unaffected. RUNX1 and RUNX3 interact with FANCD2 independently of CBFβ, suggesting a nontranscriptional role for RUNX in DNA repair. These findings suggest that RUNX dysfunction causes DNA repair defect, besides transcriptional misregulation, and promotes the development of leukemias and other cancers.

INTRODUCTION

Runx proteins belong to a family of heterodimeric transcription factors, PEBP2/CBF, that controls critical cell fate determination in several lineages (Ito, 2008) and is composed of two subunits: a DNA-binding α subunit, and a non-DNA-binding β subunit (Cbfβ). The α subunit in mammals is encoded by three Runx family genes, namely *Runx1*, *Runx2*, and *Runx3*. *RUNX1* or *AML1* is one of the most frequently mutated genes in human leukemias (Ley et al., 2013; Osato, 2004; Speck and Gilliland, 2002). *RUNX3* and *CBFB* are also shown to be associated with leukemogenesis (Liu et al., 1993; Maddipoti et al., 2008). Furthermore, recent findings showed the presence of *RUNX1* and *CBFB* mutations in breast cancer (Banerji et al., 2012) and *RUNX3* involvement in lung cancer (Lee et al., 2013).

Conditional knockout (cKO) of *Runx1* results in transient hematopoietic stem cell (HSC) expansion and subsequent exhaustion (Jacob et al., 2010; Motoda et al., 2007). *Runx3* cKO mice reveal a mild expansion of myeloid cells and HSCs when aged, partially phenocopying *Runx1* cKO mice (Wang et al., 2013b). Because Runx family genes were expected to have a compensatory mechanism, we generated hematopoietic-specific *Runx1;Runx3* double-knockout (DKO) mice. Strikingly, concurrent disruption of *Runx1* and *Runx3* resulted in mouse lethality due to bone marrow failure (BMF) or myeloproliferative disorder (MPD). Such clinically opposing manifestations are also seen in human inherited bone marrow failure syndromes (IBMFSs) that are known to be caused by defective DNA damage repair. Fanconi anemia (FA) is the most common disease constituting IBMFSs, characterized by progressive BMF and cancer predisposition, being caused by the biallelic disruption of FA gene products that participate in the repair of DNA interstrand cross-links (ICLs) (Moldovan and D'Andrea, 2009). Interestingly, FA-like clinical manifestations were recently reported in two human patients with chromosome 21q deletions in the region encompassing *RUNX1* (Byrd et al., 2011; Click et al., 2011). Because these patients did not exhibit mutations in FA genes tested, it was suggested that deletion of *RUNX1* might be the cause for FA-like clinical symptoms.

Thus, we interrogated whether the phenotypes of *Runx1;Runx3* DKO mice represented a FA-like manifestation. We show that combined ablation of *Runx1* and *Runx3* in both mice and human cell lines leads to FA phenotypes and describe a role for RUNX in the recruitment of FANCD2, a central protein of the ICL repair pathway. Interestingly, the DNA repair function of Runx is independent of Cbfβ, suggesting a nontranscriptional role of Runx in DNA repair. Our findings have unraveled a previously unappreciated intimate link between RUNX and FA.

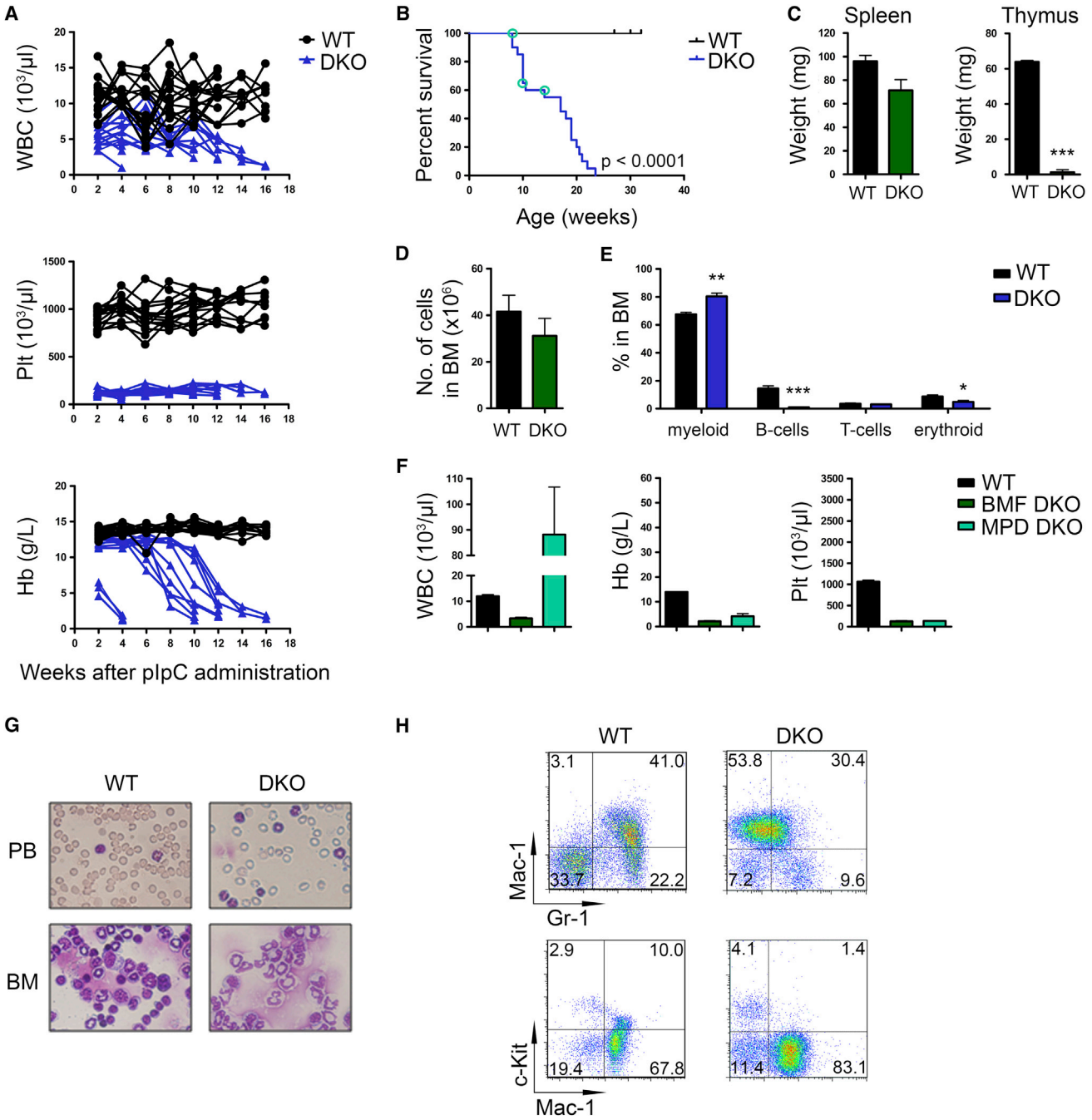

Figure 1. *Runx1;Runx3* DKO Mice Display a BMF Phenotype or MPD

(A) Time courses of WBC, Plt, and Hb counts of individual *Runx1;Runx3* WT (black lines; n = 16) and *Runx1;Runx3* DKO (blue lines; n = 14) mice are shown.

(B) Kaplan-Meier survival curves of *Runx1;Runx3* WT (black line; n = 16) and *Runx1;Runx3* DKO (blue line; n = 20) mice. The p value from Mantel-Cox test is shown. Vertical ticks and open circles represent censored cases and MPD cases, respectively.

(C) Weight of spleen (left) and thymus (right) in BMF *Runx1;Runx3* DKO mice. Mean ± SEM from four independent experiments is shown (WT, n = 4; DKO, n = 5).

(legend continued on next page)

RESULTS

Adult *Runx1;Runx3* DKO Mice Show Lethality due to BMF or MPD

To examine the effects of *Runx1* and *Runx3* ablation in the hematopoietic system, *Runx1*$^{fl/fl}$;*Runx3*$^{fl/fl}$;*Mx1-Cre*$^{+}$ and *Runx1*$^{fl/fl}$;*Runx3*$^{fl/fl}$;*Mx1-Cre*$^{-}$ mice were generated and injected with polyinosinic-polycytidylic acid (pIpC) at 4 weeks of age to induce Cre expression. Hereafter, these mice are referred to as *Runx1*;*Runx3* DKO mice and *Runx1*;*Runx3* wild-type (WT) mice, respectively. The deletion efficiency of floxed alleles after *Cre* expression was nearly complete in the bone marrow (BM) from *Runx1*;*Runx3* DKO mice (Figure S1A).

BMF Mice

Complete blood counts (CBCs) in peripheral blood (PB) were monitored fortnightly. At 4 weeks after pIpC injection, 82% (14 out of 17) of *Runx1*;*Runx3* DKO mice had decreased white blood cell (WBC) and platelet (Plt) counts, compared to WT mice (Figure 1A, top and middle panels). Moreover, *Runx1;Runx3* DKO mice developed anemia, evident from decreased hemoglobin (Hb) levels, at later time points (Figure 1A, bottom panel). These mice, termed BMF *Runx1;Runx3* DKO mice, died within 18 weeks postinduction (Figure 1B).

Necropsy of BMF *Runx1;Runx3* DKO mice revealed smaller spleen size and almost undetectable thymus (Figure 1C). BM cellularity was slightly lower in BMF *Runx1;Runx3* DKO mice than WT mice (Figure 1D). Flow cytometric examination demonstrated that before BMF development, *Runx1;Runx3* DKO mice consistently showed decreased lymphoid and erythroid populations, accompanied by a relative increase in myeloid population, as compared to WT mice (Figure 1E).

MPD Mice

Surprisingly, the remaining 18% (3 out of 17; represented by open circles in Figure 1B) of the *Runx1;Runx3* DKO mice showed high WBC counts of above 50 × 10^3/μl (Figure 1F). Flow cytometric and morphological analyses of PB and BM cells from these mice showed that high WBC counts were largely due to expanded c-Kit^{-}Sca-1^{-}Mac-1^{+}Gr-1$^{-/low}$CD44^{+} myelocytes with ring-shaped nuclei (Figures 1G and 1H). These data indicate that the *Runx1;Runx3* DKO mice succumbed to MPD or leukemia. In a transplantation assay using BM cells from a diseased mouse, leukocytosis was recapitulated only in a small number of recipient mice with a long latency. Therefore, this phenotype in *Runx1;Runx3* DKO mice is more appropriately defined as MPD, but not leukemia. Such mice are termed as MPD *Runx1;Runx3* DKO mice.

Because *Runx1;Runx3* DKO mice develop BMF or MPD only after a time lapse, *Runx1;Runx3* DKO mice at presymptomatic stage are hereafter referred to as pre-BMF/MPD mice unless otherwise stated (Figure 1I).

BMF in *Runx1;Runx3* DKO Mice Is Preceded by Paradoxical Hematopoietic Stem/Progenitor Cell Expansion due to Multiple Mechanisms, including Wnt Activation

To examine if the BMF in *Runx1;Runx3* DKO mice was due to defective hematopoietic stem/progenitor cells (HSPCs), the c-Kit^{+}Sca-1^{+}Lineage^{-} (KSL) fraction in the pre-BMF/MPD *Runx1;Runx3* DKO mice was analyzed by flow cytometry and was shown to be drastically increased in the BM and spleen (Figures 2A–2D). Gene expression profiles (GEPs) of *Runx1;Runx3* DKO KSL cells were assessed to gain an insight into the mechanism(s) underlying the drastic expansion of KSL population. Gene set enrichment analysis (GSEA) revealed that a key HSC self-renewal pathway, the Wnt pathway (Mosca et al., 2013), was activated in *Runx1;Runx3* DKO KSL cells (Figure 2E), whereas Wnt inhibitors and antagonists, such as Dkkl1 and Sfrp factors (Cain and Manilay, 2013; Wang et al., 2013a), were suppressed (Figure 2F). Wnt activation in *Runx1;Runx3* DKO cells can be conferred by the loss of direct suppression by Runx proteins (Ito et al., 2008) or by transcriptional upregulation of activators. For example, Fancl, which ubiquitinates and activates β-catenin (Dao et al., 2012), was upregulated (Figure 2G). Luciferase assay further confirmed that RUNX1 and RUNX3 suppressed the expression of Fancl in a DNA-binding- and dose-dependent manner (Figure 2H). In addition, similar to *Runx1* cKO HSCs (Motoda et al., 2007), GEPs and quantitative real-time PCR showed upregulation of *Bmi1*, another important HSC self-renewal factor.

Analysis of GEP data further demonstrated the downregulation of critical HSC niche-related factors *Cxcr4*, *Vcam-1*, and *Robo4* in *Runx1;Runx3* DKO KSL cells (data not shown). It is plausible that the loss of niche-related factors led to detachment of quiescent long-term (LT) HSCs in the niche, which in turn caused an increase of rapidly cycling short-term (ST) HSCs. Similar to *Runx1* cKO mice (Jacob et al., 2010), the weakened niche interaction is likely to be the basis for HSC expansion in *Runx1;Runx3* DKO mice. Consistently, further analysis revealed decreased LT-HSC, accompanied by increased ST-HSC, within the KSL fraction of *Runx1;Runx3* DKO mice (Figures 2I and S1B). A decrease in multipotent progenitors (MPPs) was also observed. Due to the massive expansion of *Runx1;Runx3* DKO KSL cells, frequencies of LT-HSCs and MPPs in the BM were

(D) Total BM cellularity in BMF *Runx1;Runx3* DKO mice. Mean ± SEM of number of cells in two femurs from five independent experiments is shown (WT, n = 5; DKO, n = 5).

(E) Frequencies of each lineage in BM from pre-BMF/MPD *Runx1;Runx3* DKO mice at 4–5 weeks postinduction. myeloid, Mac-1^{+} and Gr-1^{+}; B cells, B220^{+}CD19^{+}; T cells, CD3^{+}; erythroid, Ter119^{+}. Mean ± SEM from three independent experiments is shown (WT, n = 4; DKO, n = 5).

(F) WBC, Hb, and Plt counts of BMF and MPD *Runx1;Runx3* DKO mice. Mean ± SEM is shown (WT, n = 14; BMF DKO, n = 9; MPD DKO, n = 3).

(G) Representative May-Grünwald-Giemsa staining of PB and BM cells in MPD *Runx1;Runx3* DKO mice.

(H) Representative flow cytometric analysis of BM cells in MPD *Runx1;Runx3* DKO mice.

(I) Schematic diagram illustrating the phenotypes of *Runx1;Runx3* DKO mice. *Runx1*$^{fl/fl}$;*Runx3* $^{fl/fl}$;*Mx1-Cre*$^{+}$ mice (and littermate controls; not shown) were injected with pIpC. After Cre induction, these mice were termed *Runx1;Runx3* DKO mice and eventually succumbed to BMF or MPD. *Runx1;Runx3* DKO mice that have yet to develop either conditions were referred to as pre-BMF/MPD mice.

Asterisk(s) represents significant differences (*$p < 0.05$, **$p < 0.01$, ***$p < 0.001$, Student's t test). See also Figure S1.

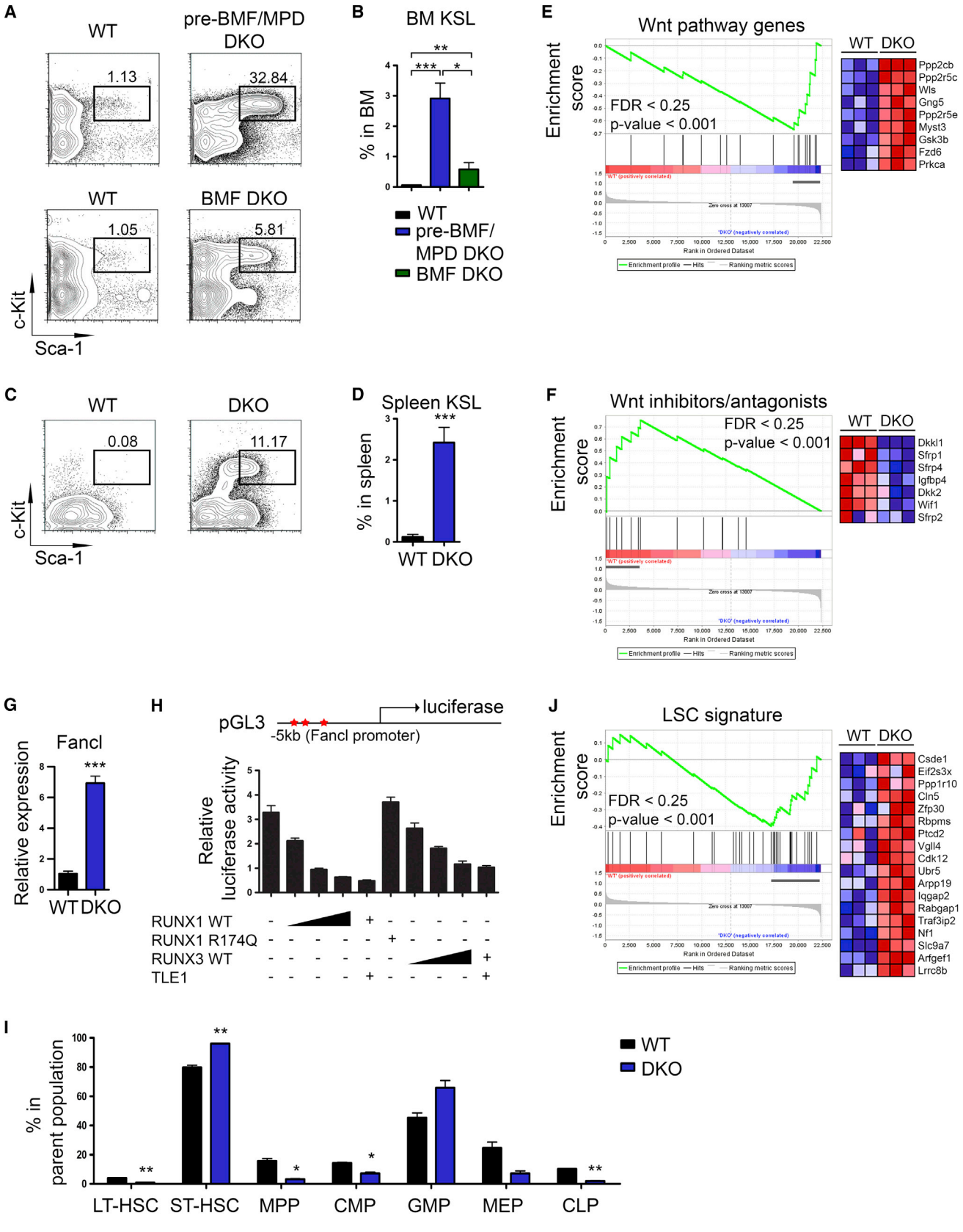

(legend on next page)

greater than WT levels (Figure S1C). Examination of specific hematopoietic progenitor compartments in the BM showed an increased granulocyte/macrophage progenitor (GMP) fraction and decreased common myeloid progenitor (CMP) and megakaryocyte/erythroid progenitor (MEP) fractions within the myeloid progenitor compartment (c-Kit$^+$Sca-1$^-$Lineage$^-$) of *Runx1;Runx3* DKO mice (Figure 2I). However, lineage priming toward GMPs was not observed in the KSL population of *Runx1;Runx3* DKO mice (data not shown). In addition, there were decreased common lymphoid progenitor (CLP) cells in the *Runx1;Runx3* DKO BM.

GSEA demonstrated significant enrichment of leukemia stem cell (LSC)-related genes (Eppert et al., 2011) in *Runx1;Runx3* DKO KSL cells (Figure 2J). Therefore, combined depletion of *Runx1* and *Runx3* appears to deregulate the core transcriptional program that controls normal and malignant stem cell behavior, including self-renewal capability, thereby contributing to the dramatic expansion of *Runx1;Runx3* DKO KSL cells.

Stem Cell Exhaustion and Differentiation Blocks across All Hematopoietic Lineages Lead to BMF in *Runx1;Runx3* DKO Mice

HSPC frequencies from BMF mice were quantified to study the contradictory phenomenon of HSPC expansion culminating into BMF. In BMF *Runx1;Runx3* DKO mice, the expansion of the BM KSL compartment significantly decreased by 5-fold ($p < 0.05$, Student's t test) from the initial 48.7-fold increase in pre-BMF/MPD *Runx1;Runx3* DKO mice, to an average of 9.6-fold increase in BMF mice (Figures 2A, bottom panel, and 2B). This progressive reduction in KSL cells indicated HSC exhaustion similar to *Runx1* cKO mice (Jacob et al., 2010).

The complete lack of blood production was too severe to be explained by HSC exhaustion alone. Therefore, *Runx1;Runx3* DKO mice were examined for additional hematopoietic defects. Flow cytometric analysis revealed significant maturation blocks in B and T cell precursors from pre-pro-B stage (B220$^+$CD43$^+$BP-1$^-$HSA$^-$) to early pro-B stage (B220$^+$CD43$^+$BP-1$^-$HSA$^+$) and within the double-negative (DN) population at the DN1 (CD44$^+$CD25$^-$) to DN2 (CD44$^+$CD25$^+$) transition (Figures 3A and 3B). An increase in CD41$^+$CD61$^+$ megakaryocytic lineage cells was observed (Figure 3C, top). However, histological analysis revealed the loss of mature megakaryocytes with large size and multinuclei concomitant with an accumulation of smaller and paired CD41$^+$ cells, indicating increased cytokinesis of megakaryoblasts in *Runx1;Runx3* DKO mice (Figure 3C, bottom). Erythroblast differentiation was blocked at the pro-E (Ter119^{int}CD71^{hi}) to EryB (Ter119^{hi}CD71^{hi}) transition (Figure 3D). Interestingly, there was a significant expansion of Mac-1$^+$Gr-1$^{-/low}$ immature granulocytes with ring-shaped nuclei in the BM of *Runx1;Runx3* DKO mice (Figure 3E). Because the expansion of immature cells was accompanied by the reduction in mature Mac-1^{hi}Gr-1^{hi} granulocytes, a blockage in terminal differentiation in granulocytes is thought to occur in *Runx1;Runx3* DKO mice. A summary of these results is provided in Figure 3F. Briefly, combined loss of *Runx1* and *Runx3* inhibits the maturation of lymphocytes, megakaryocytes, and erythrocytes at early stages of development, whereas the blockage in granulocytes was observed at a relatively late stage, accompanied by the expansion of Mac-1$^+$Gr-1$^{-/low}$ cells. We conclude that differentiation failure coupled with progressive stem cell exhaustion contributed to BMF in *Runx1*;*Runx3* DKO mice.

Differentiation Blocks, HSPC Expansion, and MPD in *Runx1;Runx3* DKO Mice Are Largely Cell Autonomous

To assess whether the phenotypes in *Runx1*;*Runx3* DKO mice were cell autonomous, bone marrow transplantations (BMTs) were conducted. Congenic strains of the pan-hematopoietic marker CD45 were used to distinguish the origins of repopulating cells (Figure 4A).

At 8 weeks post-BMT, donor chimerisms reached ~90% in the BM of recipient mice, and *Runx1*;*Runx3* DKO-transplanted mice had lower WBC, Hb, and Plt counts than *Runx1*;*Runx3* WT-transplanted mice (Figure 4B). *Runx1*;*Runx3* DKO donor cells exhibited a skewed composition toward fewer B and T cells and more myeloid cells in the PB, BM, and thymus in the recipient mice, compared to *Runx1*;*Runx3* WT donor cells (Figures 4C and 4D). *Runx1*;*Runx3* DKO donor KSL cells displayed substantial increase (Figure 4E; ~14.7-fold increase), although less remarkable as the 48.7-fold increase in the earlier-mentioned non-BMT, pre-BMF/MPD *Runx1*;*Runx3* DKO mice. The lethal phenotypes were recapitulated in *Runx1;Runx3* DKO-transplanted mice, albeit less drastic than that of the *Runx1*;*Runx3*

Figure 2. *Runx1;Runx3* DKO Mice Exhibit an Initial Expansion, but Subsequent Exhaustion, in the HSPC Compartment

(A and C) Flow cytometric analysis of the HSPC compartment in BM (A) and spleen (C) of *Runx1;Runx3* DKO mice. Representative plots gated from viable Lineage$^-$ cells of pre-BMF/MPD *Runx1*;*Runx3* DKO mice at 5 weeks postinduction (A, top panel, and C) and BMF *Runx1*;*Runx3* DKO mice (A, bottom panel) are shown. Percentages shown are frequencies of parent population.

(B and D) Graphical representations of results presented in (A) and (C) are shown in (B) and (D), respectively. Mean ± SEM of frequency of KSL in the BM (WT, n = 5; pre-BMF DKO, n = 4; BMF DKO, n = 2) (B) and spleen (n = 4/genotype) (D) is shown.

(E and F) GSEA for Wnt pathway (E) and Wnt inhibitors/antagonists (F). In the left view, an enrichment plot and ranked list for the genes are shown. Black solid bar represents leading edge genes. In the right view, a heatmap of the leading edge genes is shown. Statistical significance is given as false discovery rate (FDR) q value and p value.

(G) Quantitative real-time PCR of murine *Fancl* in BM KSL cells. Mean ± SEM of relative expression is shown (n = 3/genotype).

(H) Luciferase assay showing repression of *Fancl* gene expression by RUNX1 and RUNX3 in U937 cells. In the top view, a construct with a Fancl promoter region containing three RUNX-binding sites (red stars) was used. In the bottom view, mean ± SEM of triplicates in a representative experiment is shown. RUNX1 R174Q is a RUNX1 mutant defective in DNA binding. TLE1 is a corepressor known to function as a cofactor for RUNX-mediated transcriptional suppression.

(I) Flow cytometric analysis of individual HSPC compartments in *Runx1;Runx3* DKO mice at 5 weeks postinduction. Mean ± SEM of percentages within parent gate is shown (n = 2/genotype). Representative data from one out of two independent experiments are presented.

(J) GSEA for LSC genes. See legends for (E) and (F).

Asterisk(s) represents significant differences (*$p < 0.05$, **$p < 0.01$, ***$p < 0.001$, Student's t test). See also Figure S1.

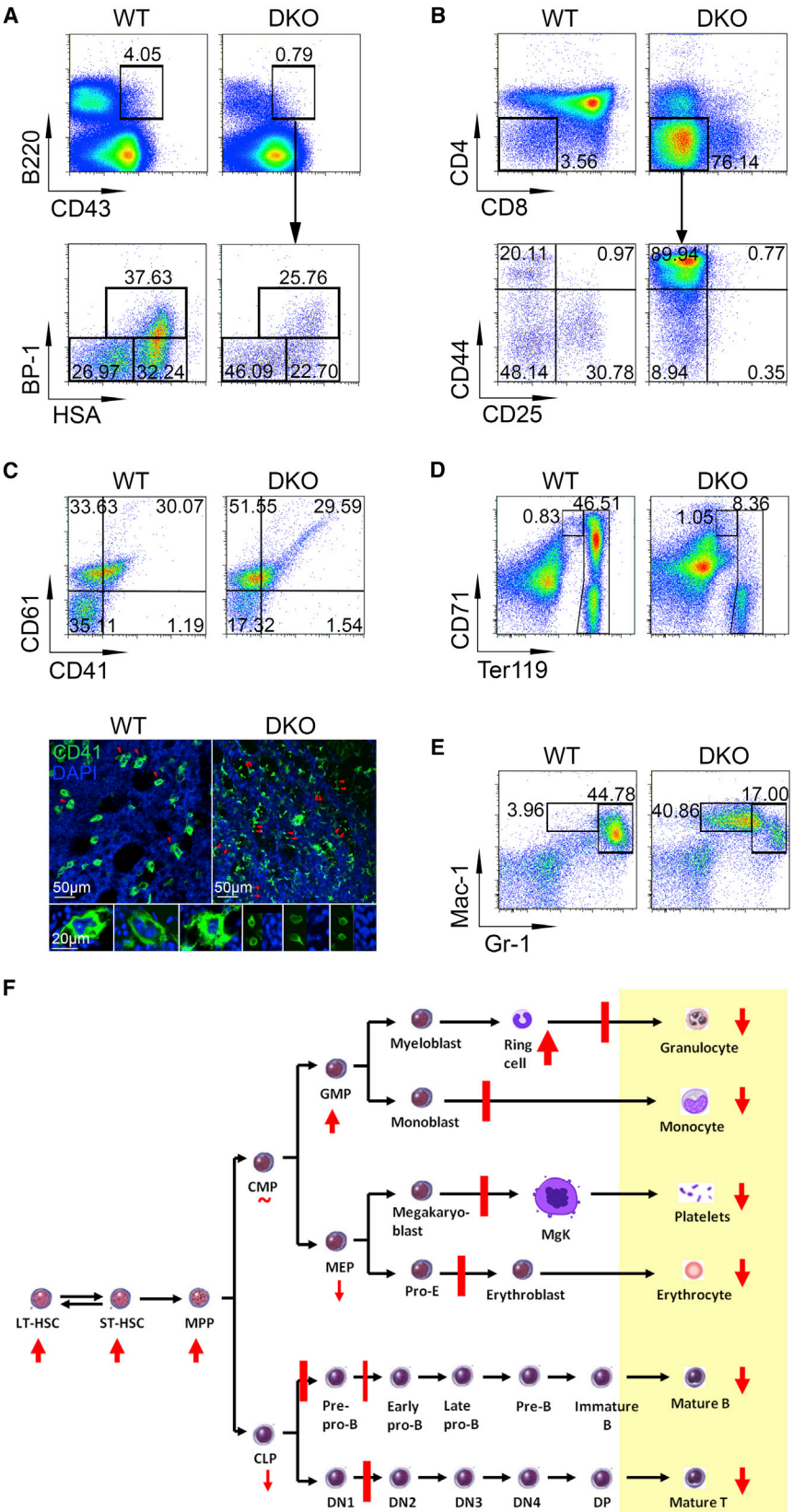

Figure 3. Differentiation Blocks Occur at Specific Developmental Stages in All Hematopoietic Lineages in *Runx1;Runx3* DKO Mice

(A and B) Flow cytometric analysis of B cell precursors in the BM (A) and T cell precursors in the thymus (B) of *Runx1;Runx3* DKO mice at 6–8 weeks postinduction. Representative plots gated from viable cells are shown. Percentages shown are frequencies of parent gate.

(C) Top, flow cytometric analysis of megakaryocytes in the BM of BMF *Runx1;Runx3* DKO mice. Representative plots gated from viable BM cells are shown. Bottom view presents histological analysis of the corresponding BMs showing $CD41^{+}$ megakaryocytes (red arrowheads). Half-bones were stained with anti-CD41 antibody (green) and DAPI (blue). Representative magnified images are depicted below.

(D and E) Flow cytometric analysis of erythroid precursors (D) and myeloid cells (E) in the BM of BMF *Runx1;Runx3* DKO mice.

(F) Schematic diagram summarizing the results shown in (A)–(E). Differentiation blocks (red lines) occurred at specific developmental stages in multiple lineages in the *Runx1;Runx3* DKO mice. The differentiation blocks ultimately led to the failure in production of mature cells of the various lineages (red arrows within yellow box). Changes in the HSPC and precursor populations are also indicated (red arrows outside yellow box).

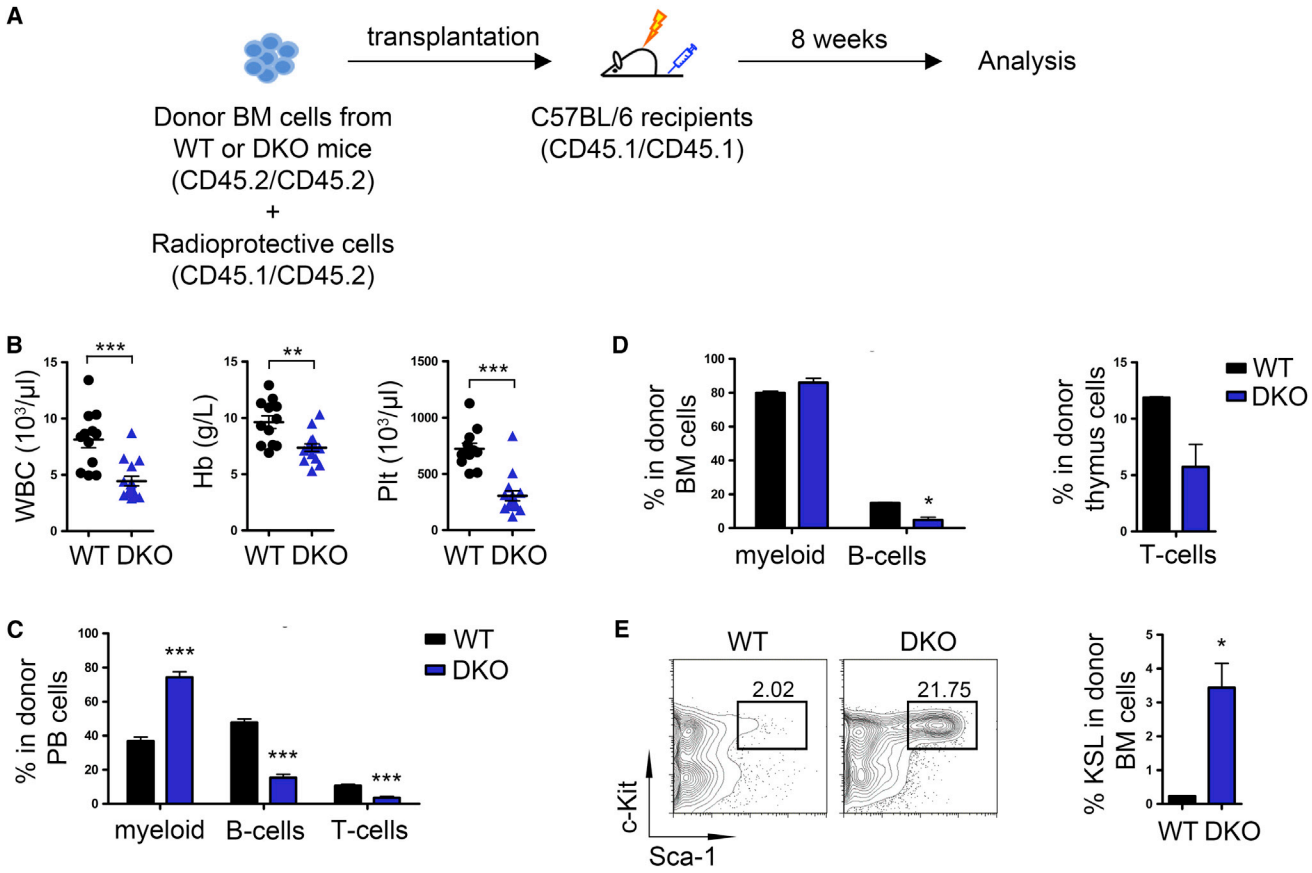

Figure 4. Differentiation Blocks and HSPC Expansion in *Runx1;Runx3* DKO Mice Are Cell Autonomous

(A) Schematic diagram showing an overview of the BMT experiment. Prior to transplantation, floxed alleles were induced for excision in *Runx1*$^{fl/fl}$;*Runx3*$^{fl/fl}$;*Mx1-Cre*$^{-}$ and *Runx1*$^{fl/fl}$;*Runx3*$^{fl/fl}$;*Mx1-Cre*$^{+}$ mice. A total of 1 × 10^{6} donor BM cells from *Runx1;Runx3* WT and *Runx1;Runx3* DKO mice (CD45.2/CD45.2) were then transplanted, with 0.2 × 10^{6} radioprotective BM cells (CD45.1/CD45.2), into sublethally irradiated C57BL/6 recipient mice (CD45.1/CD45.1). Two independent transplantations were performed.

(B) WBC, Hb, and Plt counts of transplanted mice at 8 weeks post-BMT. Mean ± SEM is shown (WT, n = 12; DKO, n = 15).

(C and D) Frequency of each lineage in CD45.2/CD45.2 donor cells in PB (C), BM (D, left), and thymus (D, right) at 8 weeks post-BMT. myeloid, Mac-1^{+} and Gr-1^{+}; B cells, B220^{+}CD19^{+}; T cells, CD3^{+}. Mean ± SEM is shown (WT, n = 13; DKO, n = 15 [C]; WT, n = 2; DKO, n = 3 [D]).

(E) Frequency of HSPCs in CD45.2/CD45.2 donor BM cells at 8 weeks post-BMT. In the left view, representative flow cytometry plots gated from viable CD45.2^{+}CD45.1^{-}Lineage^{-} cells are shown. Percentages shown are frequencies of parent gate. In the right view, mean ± SEM of frequency of KSL cells within the CD45.2^{+}CD45.1^{-} population is shown (WT, n = 2; DKO, n = 3).

Asterisk(s) represents significant differences (*p < 0.05, **p < 0.01, ***p < 0.001, Student's t test). See also Figure S2.

DKO mice because longer time was required to exhibit the phenotypes. Together, these results indicate that the BMF and MPD phenotypes in *Runx1;Runx3* DKO mice were largely cell autonomous, with a minor contribution from non-cell-autonomous factors. Results from a similar BMT experiment where donor BM cells from *Runx1*$^{fl/fl}$;*Runx3*$^{fl/fl}$;*Mx1-Cre*$^{+}$ and *Runx1*$^{fl/fl}$;*Runx3*$^{fl/fl}$;*Mx1-Cre*$^{-}$ mice were transplanted prior to pIpC treatment led to similar conclusions (Figure S2).

Absence of Runx1 and Runx3 Leads to Impaired ICL Repair

The BMF and MPD manifestations in *Runx1;Runx3* DKO mice are reminiscent of human IBMFSs, whereby two contradictory phenotypes in a single patient are caused by defective DNA repair, which leads to either eradication of unrepaired damaged cells or the accumulation of tumor-promoting genetic mutations. Therefore, *Runx1;Runx3* DKO mice were interrogated for defective DNA repair pathways leading to IBMFS. The susceptibility to DNA damage stimuli was observed as more *Runx1;Runx3* DKO mice had succumbed to total body irradiation (TBI) as compared to their WT counterparts (Figure 5A). Correspondingly, persistent γH2AX foci indicative of increased DNA damage were observed in *Runx1;Runx3* DKO KSL cells after in vitro irradiation (IR) (Figure 5B). Also, increased γH2AX+ population was detected by flow cytometry analysis (Figure S3A). Moreover, there was a greater fold reduction in the percentage of KSL fraction after TBI (Figure S3B). Micronuclei (MN), an indicator of DNA damage, showed increased accumulation in the PB cells of *Runx1;Runx3* DKO mice after TBI (Figure 5C). These results suggest that defective DNA

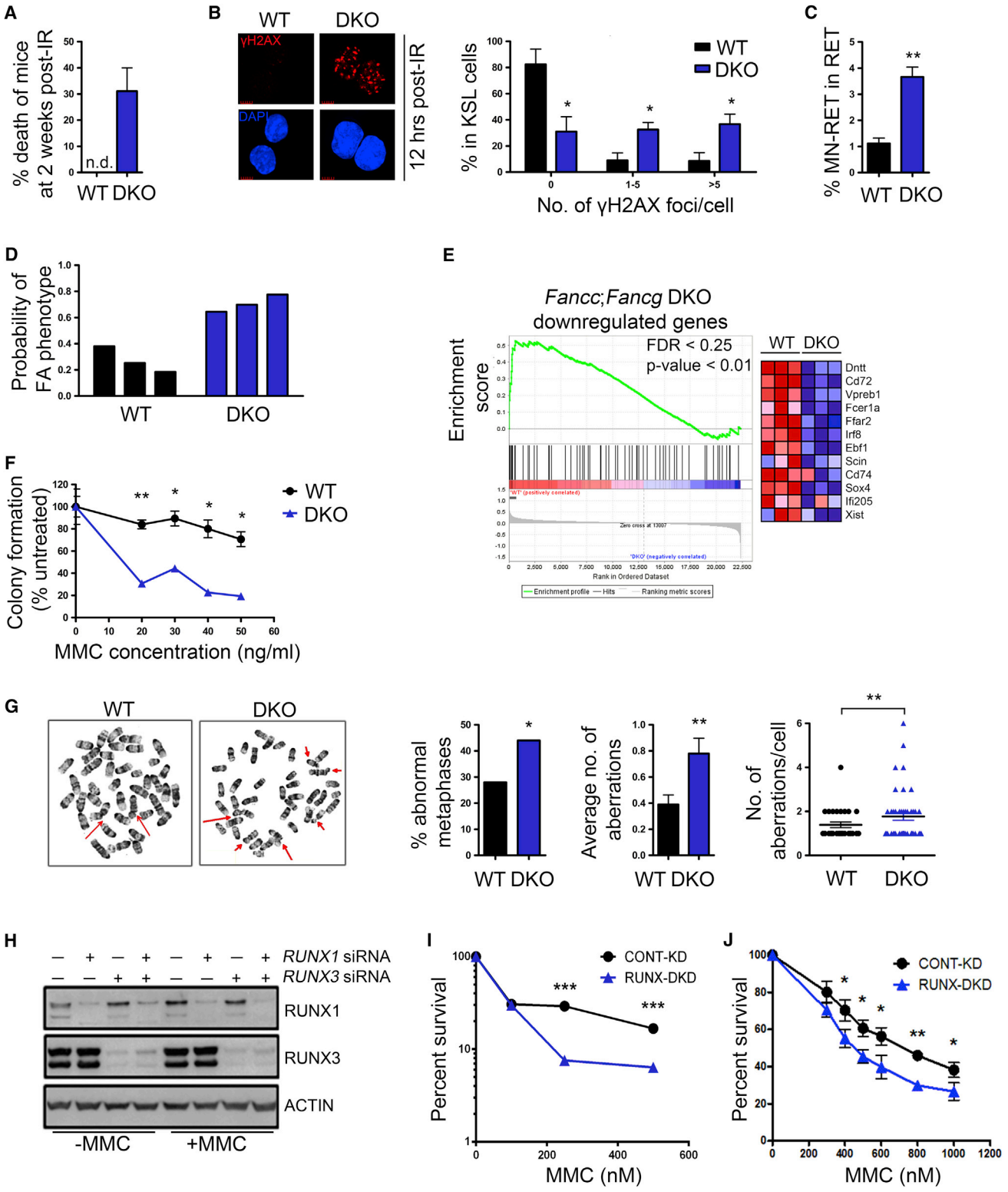

Figure 5. *Runx1;Runx3* DKO Cells Show Increased IBMFS-like Genetic Instability

(A) Survival of *Runx1;Runx3* WT (n = 11) and *Runx1;Runx3* DKO (n = 14) mice after total body IR. To avoid misinterpretation of lethality due to the spontaneous phenotypes in *Runx1;Runx3* DKO mice, we examined the effects of IR at 2 weeks post-IR. Mean ± SEM of percentage of mice that died 2 weeks after IR (5 Gy) is shown. n.d., not detectable.

(legend continued on next page)

repair in *Runx1;Runx3* DKO mice is similar to that of patients with IBMFS.

Because FA is the most common disease among the IBMFS group of diseases and recent clinical reports suggest a link between *Runx* factors and FA, GEP data sets of BM KSL fractions were analyzed to examine if *Runx1;Runx3* DKO mice resembled FA. GEP data from *Fancc*;*Fancg* DKO cells (Pulliam-Leath et al., 2010) were compared to that of *Runx1;Runx3* DKO cells. A binary regression analysis was employed to generate a FA signature based on GEP data from *Fancc*;*Fancg* WT and *Fancc*;*Fancg* DKO BM cells. In accordance to the degree of FA phenotype, *Fancc*;*Fancg* WT and *Fancc*;*Fancg* DKO mice have low and high probability, respectively, of a FA phenotype. By employing this FA signature, *Runx1;Runx3* DKO samples showed higher probability of having FA gene expression-based phenotype as compared to *Runx1;Runx3* WT samples (Figure 5D). In addition, GSEA using a gene set of downregulated genes in *Fancc*;*Fancg* DKO BM cells demonstrated a significant enrichment with the downregulated genes in *Runx1*;*Runx3* DKO samples (Figure 5E), suggesting similarity between *Runx1;Runx3* DKO mice and the FA mouse model.

Because a hallmark of FA cells is hypersensitivity to ICL-inducing agents, progenitor cells from *Runx1;Runx3* DKO mice were treated with mitomycin C (MMC). *Runx1;Runx3* DKO cells showed decreased survival upon treatment with MMC (Figure 5F), and cytogenetic analysis of treated *Runx1;Runx3* DKO cells exhibited increased chromatid and chromosomal breaks (Figure 5G), which are consistent with FA phenotype.

To recapitulate the FA-associated phenotype in other cell types, double knockdown (DKD) of *RUNX1* and *RUNX3* (*RUNX1;RUNX3* DKD) was achieved using a RNA-interference based knockdown (KD) strategy. Well-established cell lines for the study of FA, HeLa-S3, and HCT116 were used (Figure 5H). KD did not cause changes in cell viability (data not shown) or cell-cycle profiles (Figure S3C). *RUNX1;RUNX3* DKD cells showed MMC hypersensitivity (Figure 5I), increased MMC-induced chromosomal breaks (Figure S3D), and elevated accumulation of MN before and after MMC treatment (Figure S3E). Similar results were obtained in a hematopoietic cell line: Jurkat (Figure 5J). *BRCA1* KD cells were used as a positive control for the karyotype and MN analyses (Figures S3D–S3F). Therefore, FA-like manifestations observed in *Runx1;Runx3* DKO mice appear to be reproduced at least in human hematopoietic and epithelial cells tested, and they seemingly serve as a platform for further precise molecular analysis.

RUNX1 and RUNX3 Are Dispensable for FANCD2/FANCI Monoubiquitination but Essential for Full Formation of FANCD2/BRCA1 Foci

Cells deal with ICLs by activating the ATR-dependent DNA damage checkpoint. The activated FA core complex then catalyzes FANCD2/FANCI monoubiquitination through FANCL ubiquitin ligase. Monoubiquitinated FANCD2 (FANCD2-Ub) localizes to sites of ICLs and forms nuclear foci, which act as scaffold for the recruitment of downstream DNA repair proteins (Kee and D'Andrea, 2010). Notably, monoubiquitination of FANCD2 is necessary but insufficient for the formation of FANCD2 foci because FANCD2 monoubiquitination and foci formation can be uncoupled in specific contexts such as when *Brca1*, *Snm1*, or *Usp1* are knocked down (Kim et al., 2009; Mason and Sekiguchi, 2011). We interrogated four key steps of ICL repair in *RUNX1;RUNX3* DKD cells: DNA damage checkpoint, FANCD2/FANCI monoubiquitination, FANCD2 foci formation, and homologous recombination (HR) repair. Cell-cycle analysis showed that the extent of G_2/M accumulation, as well as phosphorylation of CHK1 and p53, was similar between control and *RUNX1;RUNX3* DKD samples after MMC treatment (Figures S4A and S4B), suggesting intact ATR-mediated checkpoint activation.

Data from two cell lines (HeLa-S3 and HCT116) showed a similar extent of FANCD2 and FANCI monoubiquitination,

(B) Increased DNA damage in *Runx1*;*Runx3* DKO BM cells after in vitro IR. In the left panel, pictures show representative analyses of γH2AX foci in sorted KSL cells at 12 hr after IR (4 Gy). In the right panel, mean ± SEM of results presented in the left panel is shown (WT, n = 3; DKO, n = 4).

(C) Flow cytometric analysis of micronucleated cells in the PB of *Runx1;Runx3* DKO mice. Mean ± SEM of MN-positive cells in $CD71^+$ RET population after IR (1 Gy) is shown (WT, n = 2; DKO, n = 4). Representative data from one out of two independent experiments are presented.

(D) Similarity of *Runx1*;*Runx3* DKO phenotypes with FA. Mouse FA signature is generated using binary regression analysis by comparing *Fancc*;*Fancg* WT GEPs against *Fancc*;*Fancg* DKO GEPs. The outcome of applying the FA signature on *Runx1*;*Runx3* DKO mice is shown.

(E) GSEA of *Fancc*;*Fancg* DKO BM downregulated genes using *Runx1*;*Runx3* WT and *Runx1*;*Runx3* DKO GEPs. See legends for Figures 2E and 2F.

(F) MMC sensitivity of BM myeloid progenitor cells (c-Kit^+Sca-$1^-$$Lineage^-$) from *Runx1;Runx3* WT (black) and *Runx1;Runx3* DKO (blue) mice. Mean ± SEM of colony-forming unit-culture (CFU-C) numbers, given as percentage of untreated, is shown. Representative data from one out of two independent experiments are presented.

(G) Cytogenetic analysis of *Runx1*;*Runx3* DKO BM myeloid progenitor cells. In the far-left panel, representative metaphase spreads showing MMC-induced chromatid/chromosomal breaks (red arrows) after 48 hr of MMC treatment are presented. In the left panel, the percentage of abnormal metaphases is shown (*$p < 0.05$, Fisher's exact test). In the right panel, mean ± SEM of the total number of aberrations per metaphase is shown (**$p < 0.01$, Student's t test). In the far-right panel, mean ± SEM of the number of aberrations per abnormal metaphase is shown (**$p < 0.01$, F test). Representative data from one out of two independent experiments are presented.

(H) Expression of RUNX1 and RUNX3 in *RUNX1* KD, *RUNX3* KD, and *RUNX1;RUNX3* DKD HCT116 cells. After 72 hr of siRNA treatment, cells were kept untreated or treated with 1 μM MMC for 24 hr. Western blots were probed with antibodies against RUNX1 and RUNX3.

(I) Survival of *RUNX1*;*RUNX3* DKD HCT116 cells after MMC treatment. After 72 hr of siRNA treatment, cells were treated with various doses of MMC for 24 hr in triplicates, and cell growth was measured after 5 days. Representative data from one out of three independent experiments are presented. Mean ± SEM of percent survival, given as percentage of untreated cells, is shown.

(J) Survival of *RUNX1*;*RUNX3* DKD Jurkat cells after MMC treatment. After 48 hr of siRNA treatment, cells were treated with various doses of MMC for 48 hr in triplicates, and cell viability was measured. Representative data from one out of two independent experiments are presented. Mean ± SEM of percent survival, given as percentage of untreated cells, is shown.

Asterisk(s) represents significant differences (*$p < 0.05$, **$p < 0.01$, ***$p < 0.001$, Student's t test unless otherwise stated). See also Figure S3.

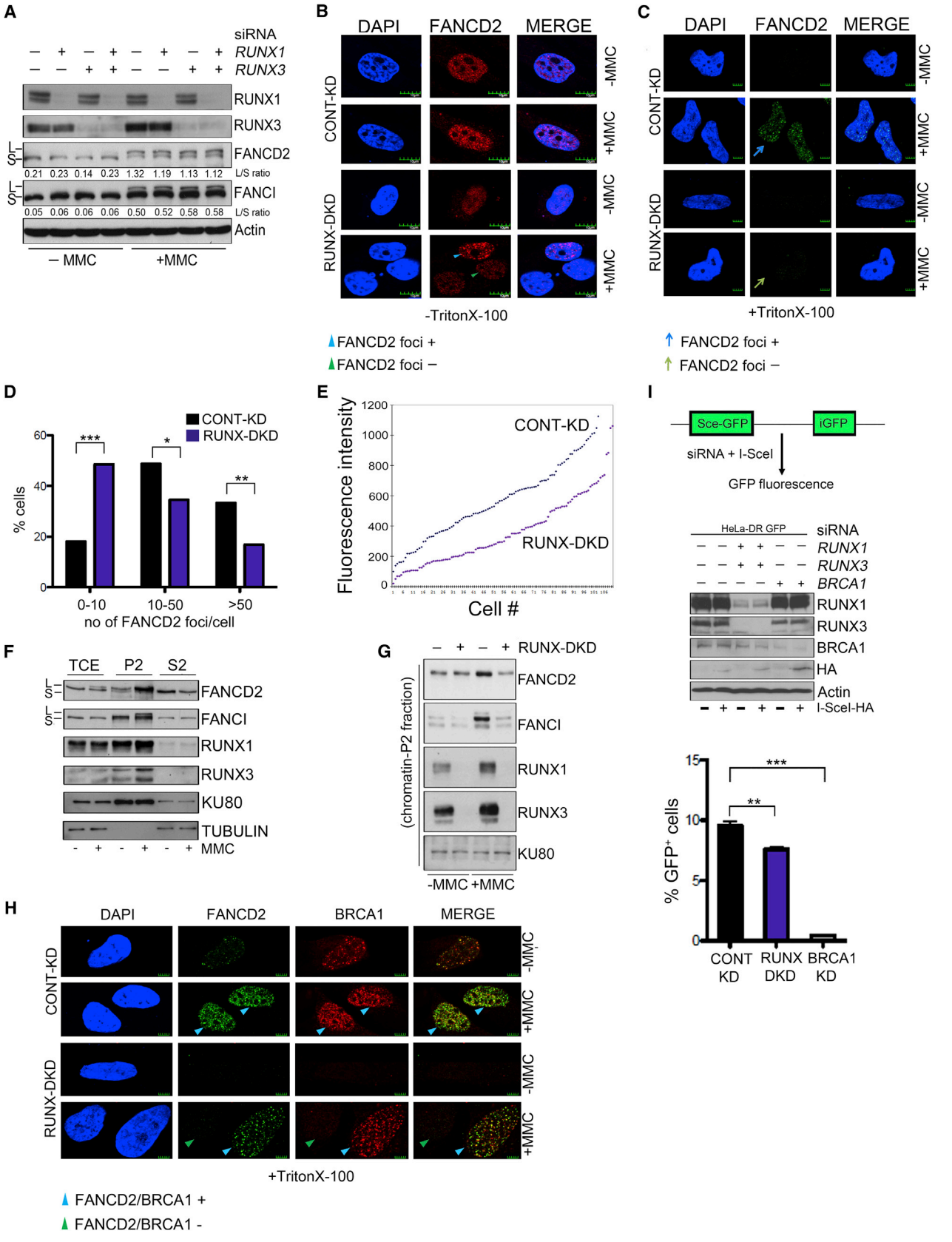

(legend on next page)

measured by the ratio of monoubiquitinated versus unmodified proteins, in *RUNX1;RUNX3* DKD and control cells after exposure to MMC (Figures 6A and S4C), suggesting intact ubiquitin ligase activity of the FA core complex. Interestingly, whereas 24 hr of MMC exposure induced robust FANCD2 foci formation in control cells, FANCD2 foci were not efficiently formed in *RUNX1;RUNX3* DKD cells (Figures 6B, 6C, and S5A). Defective FANCD2 recruitment was more discernible when Triton X-100 pre-extraction of soluble FANCD2 was performed before subsequent processing (Figure 6C). The defect was also quantified using automated image analysis software (ImageJ) (Figure 6D). The average fluorescence intensity of FANCD2 foci per cell was also reduced in *RUNX1;RUNX3* DKD cells (562 fluorescence units in control cells versus 362 fluorescence units in *RUNX1;RUNX3* DKD cells) (Figure 6E). Although some *RUNX1;RUNX3* DKD cells still retained FANCD2 foci, it seems largely not due to low transfection efficiency of small interfering RNAs (siRNAs). Using fluorochrome-labeled *RUNX1* and *RUNX3* siRNAs, transfection efficiency was determined to be higher than 92% (Figure S5B), and the RUNX proteins were significantly depleted across all cells (Figures S5C and S5D).

To independently confirm the above findings, a subcellular biochemical approach was used to assess FANCD2 recruitment (Figure S5E). Increasing amounts of FANCD2-Ub and FANCI (FANCI-Ub and unmodified form) were retained in the chromatin fractions of MMC-treated cells in a time-dependent manner (Figures 6F and S5F). Interestingly, a modest increase in RUNX1 and RUNX3 levels was noted in fraction P2 upon MMC treatment, suggesting that a portion of RUNX complexes relocates to chromatin after DNA damage (Figure 6F). Strikingly, the chromatin recruitment of FANCD2 and FANCI was significantly lower in MMC-exposed *RUNX1;RUNX3* DKD cells as compared to control cells (Figure 6G). These results confirm that the depletion of RUNX proteins leads to defective recruitment of FA proteins to sites of damage.

FANCD2 foci formation was also impaired at early time points (Figure S5G). Moreover, single depletion of *RUNX1* or *RUNX3* did not result in FANCD2 localization defects (Figure S5H). The observation that *RUNX1;RUNX3* DKD samples showed defective FANCD2 recruitment at early time points indicated that this defect might be related to an upstream signal that controls the assembly of FANCD2-Ub foci. Recent studies using *Brca1*$^{\Delta 11/\Delta 11}$ murine cells have uncovered a role for Brca1 in the control of FANCD2 foci formation during ICL repair, which is independent of its role in HR (Bunting et al., 2012). Similar to *RUNX1;RUNX3* DKD, *BRCA1* KD resulted in reduced FANCD2 foci formation (Figures S5I and S5J), although *BRCA1* depletion does not affect the preceding FANCD2 monoubiquitination step (Vandenberg et al., 2003). Upon MMC treatment of *RUNX1;RUNX3* DKD cells, all cells deficient for FANCD2 foci were concurrently defective for BRCA1 foci formation (Figures 6H and S5K).

To study if *RUNX1;RUNX3* DKD led to downstream defects in HR, the direct repeat-GFP (DR-GFP) reporter assay was used. Transient expression of the rare-cutting endonuclease, I-SceI, leads to double-strand breaks, and subsequent HR repair of the breaks results in GFP$^+$ cells that are quantifiable by flow cytometry (Figure 6I, top). Because *RUNX1;RUNX3* DKD cells have a defect at the level of FANCD2 foci formation, the extent of HR repair decreased by a mild ~30% (Figure 6I). This phenotype is similar to the moderate defect in HR observed upon ablation of core FA genes (Nakanishi et al., 2005; Yamamoto et al., 2005). In contrast, consistent with an essential role of BRCA1 in HR, GFP positivity was drastically reduced by 90% in *BRCA1* KD cells.

RUNX1 and RUNX3 Control FANCD2 Recruitment to Sites of ICLs in a Cbfβ-Independent Manner

Heterodimerization of Runx with Cbfβ is required for the protein stability and transcriptional activities of Runx. Because GEP analysis of *Runx1;Runx3* DKO cells did not reveal obvious

Figure 6. FANCD2 Foci Formation Is Defective in *RUNX1;RUNX3*-Depleted Cells

(A) FANCD2/FANCI monoubiquitination in *RUNX1* KD, *RUNX3* KD, and *RUNX1;RUNX3* DKD (RUNX DKD) HeLa-S3 cells. After 48 hr of siRNA treatment, cells were exposed to 150 nM MMC for 24 hr. Western blots were probed with indicated antibodies. L, long/monoubiquitinated form; S, short/unmodified protein.

(B and C) Immunofluorescence detection of FANCD2 foci in *RUNX1;RUNX3* DKD HeLa-S3 cells. After 48 hr of ON-TARGET plus SMARTpool siRNA treatment, cells were treated with 150 nM MMC for 24 hr before fixing (B) or pre-extracted with Triton X-100 (C). Blue arrowhead/arrow indicates FANCD2 foci+ cell (more than ten foci/cell), whereas green arrowheads/arrow indicates FANCD2 foci− cells. Scale bar, 5 μm.

(D and E) Immunofluorescence detection of FANCD2 foci in *RUNX1;RUNX3* DKD HeLa-S3 cells. HeLa-S3 cells cotransfected with TAMRA-*RUNX1* and DY647-*RUNX3* siRNA oligonucleotides were plated on coverslips, exposed to MMC for 24 hr, pre-extracted with 0.5% Triton X-100, and stained with antibody against FANCD2. Images were captured and subjected to quantitative analysis by ImageJ to measure the number of FANCD2 foci/cell (D) or average fluorescence intensity of foci/cell (E).

(F) Subcellular biochemical fractionation of HeLa-S3 cells treated with MMC. Cells were exposed to MMC, and total cell extracts (TCE) were either prepared or processed further for biochemically distinct two fractions, namely chromatin-enriched P2 and cytosolic/nucleoplasmic S2 fractions. Western blots were probed with antibodies against KU80 or Tubulin as the loading control.

(G) Chromatin fractionation of FANCD2 and FANCI in *RUNX1;RUNX3* DKD HeLa-S3 cells. After 24 hr of ON-TARGET plus SMARTpool siRNA treatment, cells were treated with 150 nM MMC for 24 hr, and chromatin-enriched fractions were isolated. Western blots were probed with indicated antibodies.

(H) Immunofluorescence detection of BRCA1 and FANCD2 foci in *RUNX1;RUNX3* DKD HeLa-S3 cells. At 48 hr after ON-TARGET plus SMARTpool siRNA treatment, cells were treated with 150 nM MMC for 24 hr before pre-extraction with 0.25% Triton X-100 and fixation. Blue arrows indicate cells that are positive for both FANCD2 and BRCA1 foci formation (FANCD2/BRCA1 foci+), whereas green arrows indicate cells that are negative for foci formation (FANCD2/BRCA1 foci−). Scale bar, 5 μm.

(I) Measurement of HR in *RUNX1;RUNX3* DKD and *BRCA1* KD HeLa cells using DR-GFP assay. Top view shows a schematic diagram depicting the DR-GFP assay. Middle view shows a western blot analysis of RUNX1, RUNX3, and BRCA1. In the bottom view, mean ± SEM of percentage of GFP$^+$ cells at 72 hr after I-SceI expression is shown.

Asterisk(s) represents significant differences (*$p < 0.05$, **$p < 0.01$, ***$p < 0.001$, Student's t test). See also Figures S4 and S5.

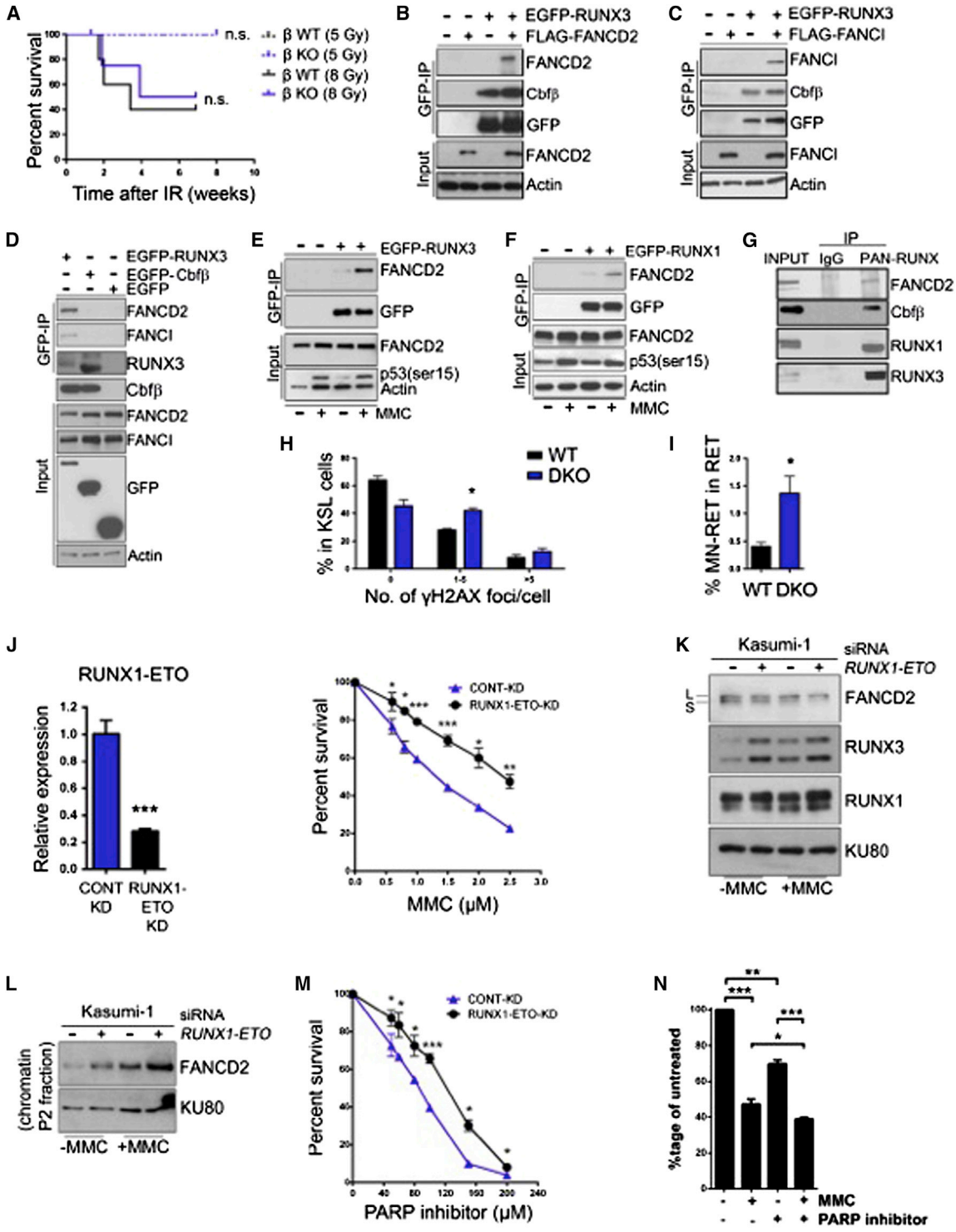

Figure 7. Interaction of RUNX1 and RUNX3 with FANCD2 Is Enhanced after MMC Treatment

(A) Kaplan-Meier survival curves of *Cbfb* WT (black dotted line, 5 Gy, n = 12; black solid line, 8 Gy, n = 11) and *Cbfb* KO (blue dotted line, 5 Gy, n = 9; blue solid line, 8 Gy, n = 8) mice after total body IR. n.s. indicates not statistically significant p value using Mantel-Cox test. Vertical ticks represent censored cases.

(B and C) Coimmunoprecipitation of FANCD2 and FANCI with RUNX3 in HEK293T cells. EGFP-RUNX3 was overexpressed with FLAG-FANCD2 (B) or FLAG-FANCI (C). Lysates were coimmunoprecipitated using GFP beads, and western blots were probed with indicated antibodies.

(legend continued on next page)

transcriptional changes in DNA repair pathways (Callen et al., 2013) (Figures S6A and S6B), we predicted that Runx1 and Runx3 may function in a nontranscriptional capacity in DNA damage response. In that case, although Runx-mediated transcription would be largely abolished in *Cbfb* KO mouse, exposure to DNA-damaging agents may not render a DNA damage sensitivity phenotype. We generated *Cbfb* cKO mice in which the deletion efficiency of floxed alleles after pIpC treatment was nearly complete in the BM (Figure S6C). In contrast to *Runx1;Runx3* DKO mice, *Cbfb* cKO mice did not show increased sensitivity to TBI compared to *Cbfb* WT mice (Figure 7A). Moreover, *Cbfb* cKO mice did not develop BMF or MPD (n = 9, 8 months old), although other phenotypes, namely HSPC expansion and differentiation blocks (unpublished data), were similar to the *Runx1;Runx3* DKO mice. Because *Cbfb* ablation largely abolishes the transcriptional activity of all Runx proteins, the above observation strongly suggests that RUNX may function in DNA repair through mechanisms distinct from its canonical transcriptional role.

Independent from the above-mentioned experiments, quantitative mass spectrometric analysis to discover RUNX3-interacting proteins identified FANCI as one of the high-confidence interactors (unpublished data). We examined whether RUNX can exercise its nontranscriptional role in DNA repair by physically associating with FANCD2-containing complexes. RUNX3 coimmunoprecipitated with exogenous and endogenous FANCD2 and FANCI (Figures 7B–7D), whereas Cbfβ failed to do so, although it interacted with endogenous RUNX3 (Figure 7D), suggesting that Cbfβ was not incorporated into such DNA repair complexes. Similar results were obtained for RUNX1. These data suggest that the fraction of RUNX that exists in a complex with FANCD2 is mutually exclusive from the RUNX/Cbfβ complex.

To study if MMC treatment stimulated the interaction of RUNX1 and RUNX3 to FANCD2, subnuclear distribution of these proteins was examined. Upon MMC treatment, a fraction of RUNX1 foci colocalized with FANCD2 foci (Figure S6D). Because most RUNX proteins are localized to transcription-associated nuclear matrix foci (Zaidi et al., 2002), it was difficult to correctly estimate the percentage of colocalization with FANCD2 foci. However, coimmunoprecipitation assays clearly revealed an increased association between RUNX3 and FANCD2 after MMC treatment (Figures S6E and S6F). Identical results were obtained when the association of overexpressed RUNX3 or RUNX1 with endogenous FANCD2 was examined after exposure to MMC (Figures 7E and 7F). Physiological relevance of RUNX-FANCD2 interaction was further ascertained by endogenous immunoprecipitation of RUNX1/RUNX3/FANCD2 complexes from MMC-exposed nuclear extracts of Jurkat cells (Figure 7G). Consistent with Cbfβ-independent interaction between RUNX and FANCD2, Cbfβ does not bind to FANCD2 even after exposure with MMC (Figure S6G).

We conclude that defective DNA repair contributes to the lethal phenotypes in *Runx1;Runx3* DKO mice. This was confirmed by increased basal levels of DNA damage in *Runx1;Runx3* DKO cells as assessed by increased γH2AX staining in BM cells (Figure 7H) and increased MN in PB reticulocytes (RETs) (Figure 7I).

RUNX1-ETO Fusion Protein Causes the Defect in the FA DNA Damage Repair Pathway

Finally, we studied the clinical relevance of RUNX participation in DNA damage repair using hematopoietic cell lines carrying RUNX alteration. Kasumi-1 is a *RUNX1-ETO* fusion gene-expressing human leukemic cell line, in which the fusion protein

(D) Coimmunoprecipitation of endogenous FANCD2 and FANCI with RUNX3, but not Cbfβ, in HEK293T cells. GFP-tagged Cbfβ, EGFP-tagged RUNX3, or empty EGFP-expressing plasmids were overexpressed in HEK293T. Lysates were coimmunoprecipitated using GFP beads, and western blots were probed with indicated antibodies.

(E and F) Coimmunoprecipitation of endogenous FANCD2 with RUNX3 and RUNX1 is enhanced after MMC treatment in HEK293T cells. EGFP-RUNX3 (E) or EGFP-RUNX1 (F) was overexpressed and left untreated or exposed to 1 μM MMC. Cell lysates were coimmunoprecipitated using GFP beads, and western blots were probed with indicated antibodies. Blots were probed for phosphorylation of p53 (ser15) as an indicator of MMC addition.

(G) Coimmunoprecipitation of endogenous FANCD2 with endogenous RUNX1 and RUNX3. Nuclear extracts isolated from Jurkat cells were treated with 0.5 μM MMC for 16 hr. Coimmunoprecipitation was performed by incubating 1 mg of nuclear extract with anti-RUNX antibody for 4 hr at 4°C. Western blots were probed with indicated antibodies.

(H) Increased DNA damage in *Runx1;Runx3* DKO BM cells without DNA damage stimulation. Mean ± SEM of percentage of KSL cells with indicated numbers of γH2AX foci is shown (n = 2/genotype).

(I) Flow cytometric analysis of micronucleated cells in the PB of *Runx1;Runx3* DKO mice without DNA damage stimulation. Mean ± SEM of MN-positive cells in RET population is shown (n = 2/genotype). Representative data from one out of two independent experiments are presented.

(J) Survival of *RUNX1-ETO* KD Kasumi-1 cells after MMC treatment. In the left panel, after 48 hr of siRNA treatment, cells were harvested for quantitative real-time PCR analysis. Mean ± SEM of RUNX1-ETO expression is shown. In the right panel, cells were treated with various doses of MMC for 48 hr, and cell viability was measured. Representative data from one out of two independent experiments are presented. Mean ± SEM of percent survival, given as percentage of untreated cells, is shown.

(K) FANCD2 monoubiquitination in *RUNX1-ETO* KD Kasumi-1 cells. After 24 hr of siRNA treatment, cells were exposed to 2 μM MMC for 24 hr, and total cell extracts were prepared. Western blots were probed with indicated antibodies. Representative data from one out of two independent experiments are presented. L, long/monoubiquitinated form; S, short/unmodified protein.

(L) FANCD2 in chromatin fraction from *RUNX1-ETO* KD Kasumi-1 cells. After 24 hr of siRNA treatment, cells were treated with 2 μM MMC for 24 hr, and chromatin-enriched fractions (P2) were isolated. Western blots were probed with indicated antibodies. Representative data from one out of two independent experiments are presented.

(M) Survival of *RUNX1-ETO* KD Kasumi-1 cells after PARP inhibitor treatment. Cells were treated with various doses of Olaparib for 48 hr, and cell viability was measured. Mean ± SEM of percent survival, given as percentage of untreated cells, is shown.

(N) Survival of Kasumi-1 cells after single or combined treatment with MMC and PARP inhibitor. Cells were treated with 1.5 μM MMC and/or 20 μM Rucaparib for 48 hr, and cell viability was measured. Mean ± SEM of percent survival, given as percentage of untreated cells, is shown.

Asterisk(s) represents significant differences (*$p < 0.05$, **$p < 0.01$, ***$p < 0.001$, Student's t test). See also Figure S6.

is thought to suppress the expression and/or function of both RUNX1 and RUNX3 simultaneously. Thus, the expression of RUNX1-ETO is expected to cause defective DNA damage repair and a DNA damage-hypersensitive phenotype. We confirmed that Kasumi-1 cells were indeed sensitive to MMC, and the KD of *RUNX1-ETO* reduced this sensitivity (Figure 7J). Similar behavior was seen in another RUNX1-ETO-expressing leukemic cell line: SKNO-1 (data not shown). Moreover, whereas FANCD2 monoubiquitination remained unaffected (Figure 7K), depletion of RUNX1-ETO led to increased FANCD2 recruitment to chromatin both in the absence and presence of MMC (Figure 7L). The above results suggest that RUNX1-ETO might repress FANCD2 foci formation and ICL repair in human leukemic cells.

One of the outcomes of FA pathway abnormality is defective HR repair, which in turn becomes addicted to alternative DNA repair pathways, such as nonhomologous end-joining and base excision repair (BER). It was hence predicted that RUNX dysfunction would sensitize cells to inhibition of BER-mediating PARP-1 (Carey and Sharpless, 2011; Ellisen, 2011). Thus, Kasumi-1 cells were treated with two PARP inhibitors: Olaparib or Rucaparib. Parental Kasumi-1 cells were more sensitive to PARP inhibitor, and the KD of *RUNX1-ETO* partially reduced this sensitivity (Figure 7M; data not shown). The efficacy of PARP inhibitor was further accentuated when cells were treated with MMC, indicating that the synthetic lethal effects of PARP-1 inhibition and MMC exposure could potentially be considered for targeting RUNX leukemia (Figure 7N).

DISCUSSION

The functional redundancy between *Runx1* and *Runx3* was unveiled by the lethality in *Runx1;Runx3* DKO mice due to BMF, caused by multiple differentiation blocks and stem cell exhaustion, or preleukemic condition, MPD, which were not observed in the respective single cKO mice (*Runx1* cKO, n = 36; *Runx3* cKO, n = 35). We found that *Runx1* and *Runx3* play important roles in DNA repair, particularly the FA pathway where RUNX proteins facilitate the recruitment of FANCD2-Ub to sites of DNA damage (Figure S7). This report illustrates a direct relationship between Runx family genes and the FA pathway. The property of Runx1 and Runx3 in the FA pathway is independent of their roles as transcription factors and appears to be a basis for the antitumorigenic roles of Runx in leukemia and solid tumor development.

The simultaneous occurrence of the two contradictory manifestations, BMF and MPD, in *Runx1;Runx3* DKO mice was reminiscent of human IBMFS. Of the several types of IBMFSs, we focused on FA because recent reports described that chromosome 21q deletion containing *RUNX1* was found in two FA-like patients. Using multiple approaches, we showed that ablation of both *Runx1* and *Runx3* led to defective DNA repair. These results suggest that *RUNX1* deletion might predispose the patients to FA-like conditions. Just as compound deficiency of *Runx3* in addition to *Runx1* was required for the FA-like phenotypes in mice, additional genetic change(s) besides *RUNX1* malfunction is also considered to be required for the manifestation of FA-like conditions in the human patients. *SOD1*, located within the deleted chromosome 21q region, seems to be an interesting candidate. *SOD1* encodes a superoxide dismutase to detoxify reactive oxygen species (ROS). Notably, SOD1 is suppressed in FA cells, causing their hypersensitivity to oxidants and MMC (Kumari et al., 2014). Identification of the deleted gene(s) responsible for the FA-like phenotypes would provide us with profound insights into RUNX function in the FA pathway. Recent technological advances have shown frequent deletions of chromosome 21q, including the *RUNX1* locus, in patients with congenital syndromic thrombocytopenia with leukemia predisposition. We propose that FA-like cellular features should be investigated in the patients with syndromic thrombocytopenia.

Although *Runx1;Runx3* DKO mice recapitulated FA phenotypes, some discordances exist between *Runx1;Runx3* DKO mice and FA patients/mouse models. The HSC compartment is usually decreased in FA but showed a massive expansion before subsequent decline in the pre-BMF/MPD *Runx1;Runx3* DKO mice. Therefore, the reasons for the HSC expansion were extensively sought in *Runx1;Runx3* DKO mice and were shown to be attributable to multiple mechanisms, including (1) increased HSC self-renewal capability due to the elevation of Bmi1 and activation of the Wnt pathway, (2) the detachment from niches responsible for HSC quiescence, and (3) increased expression of LSC-associated genes. All of these abnormalities, which are unlikely to be present in the cells of patients with FA, seem to clarify the differences in HSC compartments. Alternatively, it is possible that, at an early time point before clinical onset of BMF, IBMFS patients or mouse models may show HSC expansion to some extent as a compensatory increase in response to loss of mature hematopoietic cells and subsequent increased cytokine secretion as homeostatic machinery. This kinetics scenario has not been carefully examined in human patients or mouse models in earlier studies. Interestingly, one of the FA mouse models, *Usp1* KO mice, showed an increase in the size of its HSC compartment (Parmar et al., 2010). *Usp1* encodes ubiquitin-specific peptidase 1, a ubiquitin-specific protease that serves to deubiquitinate the FANCD2/FANCI heterodimer. Therefore, the level of Fancd2-Ub was enhanced in *Usp1* KO mice. However, Fancd2 foci formation was abrogated, resulting in MMC hypersensitivity of *Usp1* KO cells. These similarities in key phenotypes between *Usp1* KO and *Runx1;Runx3* DKO mice may help to further dissect RUNX functions in the FA pathway.

RUNX1 is among the most prevalent leukemia genes, and *RUNX3* is also associated with human leukemias. Notably, simultaneous suppression of the expression and/or function of both RUNX1 and RUNX3 was shown in acute myeloid leukemia with t(8;21) or inv(16) due to the fusion proteins (Cheng et al., 2008; Meyers et al., 1996). Therefore, the DNA damage response defects seen in *Runx1;Runx3* DKO mice may also be the mechanistic basis for leukemogenesis in common human RUNX leukemias. Our results clearly demonstrated that human leukemia cell lines expressing the *RUNX1-ETO* fusion gene are sensitive to MMC, at least partially in a fusion gene-dependent manner. This sensitivity was further enhanced in the presence of PARP inhibitor. This treatment with PARP inhibitors, together with DNA ICL and/or standard chemotherapy drugs, could be applied for RUNX leukemia. Because deregulation in RUNX family genes

is now found in a wide spectrum of cancers, this combined therapy can potentially be extended to common cancers.

EXPERIMENTAL PROCEDURES

Mice

Runx1$^{fl/fl}$ (Taniuchi et al., 2002), *Runx3*$^{fl/fl}$, *Cbfb*$^{fl/fl}$ (Naoe et al., 2007), and *Mx1-Cre*$^{+}$ mice were backcrossed to mice in the C57BL/6 background for at least three generations before being used for subsequent crosses. Animals carrying both floxed *Runx1* (*Runx1*$^{fl/fl}$) and floxed *Runx3* (*Runx3*$^{fl/fl}$) alleles were crossed with a *Mx1-Cre* transgenic line to obtain *Runx1*$^{fl/fl}$;*Runx3*$^{fl/fl}$;*Mx1-Cre*$^{+}$ mice and *Runx1*$^{fl/fl}$;*Runx3*$^{fl/fl}$;*Mx1-Cre*$^{-}$ littermate controls on the C57BL/6 background. *Cbfb*$^{fl/fl}$;*Mx1-Cre*$^{+}$ mice were obtained from similar crosses. All animal experiments followed the guidelines set by the National Advisory Committee for Laboratory Animal Research.

Cell Lines, Plasmids, and Transfection

Human embryonic kidney 293T (HEK293T), HCT116, and HeLa-S3 cell lines were procured from American Type Culture Collection. Cells were cultured by supplementing Dulbecco's modified Eagle's medium with 10% fetal bovine serum. Plasmids encoding human FLAG-RUNX3, EGFP-RUNX3, EGFP-RUNX1, and mouse EGFP-Cbfβ were described earlier by Chuang et al. (2012) and Yano et al. (2006), and a plasmid-encoding mouse FLAG-Cbfβ was constructed for the current study. HA-FLAG-tagged FANCI and FLAG-FANCD2 were kindly provided by A. Smogorzewska and N. Matsushit, respectively. HeLa-S3 stably integrated with DR-GFP was a kind gift from J. Parvin. For overexpression experiments in HEK293T, TransIT-293 transfection reagent was used according to the manufacturer's instructions.

ACCESSION NUMBERS

Microarray data are deposited in NCBI Gene Expression Omnibus under the accession number GSE51107.

SUPPLEMENTAL INFORMATION

Supplemental Information includes Supplemental Experimental Procedures and seven figures and can be found with this article online at http://dx.doi.org/10.1016/j.celrep.2014.06.046.

AUTHOR CONTRIBUTIONS

C.Q.W., V.K., and L.S.T. designed research, analyzed data, and wrote the manuscript. D.W.L.C., C.P.K., J.Y.C., G.S.S.N., L.D., B.J., N.Y., and S.K.L. performed experiments. T.Z.T. and S.M. analyzed data. I.T. provided research tools. V.T., Y.I., and M.O. designed research, analyzed data, and wrote the manuscript. All authors reviewed and approved the manuscript.

ACKNOWLEDGMENTS

The authors thank L.Q. Chen, M. Mok, and C. Chung for their technical assistance; the Biological Resource Center, Biopolis, MD2 Vivarium, and NUS for mouse husbandry; S.S. Lim, W.Y. Chua, V. Cacheux, and S. Davila from Genome Institute of Singapore for cytogenetics analysis; S.Y. Lee from NUS confocal microscopy unit for image analysis; and K. Rajewsky, N. Matsushita, A. Smogorzewska, J. Parvin, and A. Lyakhovich for experimental materials. This work was supported by A*STAR, Biomedical Research Council, National Medical Research Council, the National Research Foundation Singapore, and the Singapore Ministry of Education under its Research Centers of Excellence initiative.

Received: November 21, 2013
Revised: May 2, 2014
Accepted: June 23, 2014
Published: July 24, 2014

REFERENCES

Banerji, S., Cibulskis, K., Rangel-Escareno, C., Brown, K.K., Carter, S.L., Frederick, A.M., Lawrence, M.S., Sivachenko, A.Y., Sougnez, C., Zou, L., et al. (2012). Sequence analysis of mutations and translocations across breast cancer subtypes. Nature *486*, 405–409.

Bunting, S.F., Callén, E., Kozak, M.L., Kim, J.M., Wong, N., López-Contreras, A.J., Ludwig, T., Baer, R., Faryabi, R.B., Malhowski, A., et al. (2012). BRCA1 functions independently of homologous recombination in DNA interstrand crosslink repair. Mol. Cell *46*, 125–135.

Byrd, R.S., Zwerdling, T., Moghaddam, B., Pinter, J.D., and Steinfeld, M.B. (2011). Monosomy 21q22.11-q22.13 presenting as a Fanconi anemia phenotype. Am. J. Med. Genet. A. *155A*, 120–125.

Cain, C.J., and Manilay, J.O. (2013). Hematopoietic stem cell fate decisions are regulated by Wnt antagonists: comparisons and current controversies. Exp. Hematol. *41*, 3–16.

Callen, E., Di Virgilio, M., Kruhlak, M.J., Nieto-Soler, M., Wong, N., Chen, H.T., Faryabi, R.B., Polato, F., Santos, M., Starnes, L.M., et al. (2013). 53BP1 mediates productive and mutagenic DNA repair through distinct phosphoprotein interactions. Cell *153*, 1266–1280.

Carey, L.A., and Sharpless, N.E. (2011). PARP and cancer—if it's broke, don't fix it. N. Engl. J. Med. *364*, 277–279.

Cheng, C.K., Li, L., Cheng, S.H., Lau, K.M., Chan, N.P., Wong, R.S., Shing, M.M., Li, C.K., and Ng, M.H. (2008). Transcriptional repression of the RUNX3/AML2 gene by the t(8;21) and inv(16) fusion proteins in acute myeloid leukemia. Blood *112*, 3391–3402.

Chuang, L.S., Lai, S.K., Murata-Hori, M., Yamada, A., Li, H.Y., Gunaratne, J., and Ito, Y. (2012). RUNX3 interactome reveals novel centrosomal targeting of RUNX family of transcription factors. Cell Cycle *11*, 1938–1947.

Click, E.S., Cox, B., Olson, S.B., Grompe, M., Akkari, Y., Moreau, L.A., Shimamura, A., Sternen, D.L., Liu, Y.J., Leppig, K.A., et al. (2011). Fanconi anemia-like presentation in an infant with constitutional deletion of 21q including the RUNX1 gene. Am. J. Med. Genet. A. *155A*, 1673–1679.

Dao, K.H., Rotelli, M.D., Petersen, C.L., Kaech, S., Nelson, W.D., Yates, J.E., Hanlon Newell, A.E., Olson, S.B., Druker, B.J., and Bagby, G.C. (2012). FANCL ubiquitinates β-catenin and enhances its nuclear function. Blood *120*, 323–334.

Ellisen, L.W. (2011). PARP inhibitors in cancer therapy: promise, progress, and puzzles. Cancer Cell *19*, 165–167.

Eppert, K., Takenaka, K., Lechman, E.R., Waldron, L., Nilsson, B., van Galen, P., Metzeler, K.H., Poeppl, A., Ling, V., Beyene, J., et al. (2011). Stem cell gene expression programs influence clinical outcome in human leukemia. Nat. Med. *17*, 1086–1093.

Ito, Y. (2008). RUNX genes in development and cancer: regulation of viral gene expression and the discovery of RUNX family genes. Adv. Cancer Res. *99*, 33–76.

Ito, K., Lim, A.C., Salto-Tellez, M., Motoda, L., Osato, M., Chuang, L.S., Lee, C.W., Voon, D.C., Koo, J.K., Wang, H., et al. (2008). RUNX3 attenuates beta-catenin/T cell factors in intestinal tumorigenesis. Cancer Cell *14*, 226–237.

Jacob, B., Osato, M., Yamashita, N., Wang, C.Q., Taniuchi, I., Littman, D.R., Asou, N., and Ito, Y. (2010). Stem cell exhaustion due to Runx1 deficiency is prevented by Evi5 activation in leukemogenesis. Blood *115*, 1610–1620.

Kee, Y., and D'Andrea, A.D. (2010). Expanded roles of the Fanconi anemia pathway in preserving genomic stability. Genes Dev. *24*, 1680–1694.

Kim, J.M., Parmar, K., Huang, M., Weinstock, D.M., Ruit, C.A., Kutok, J.L., and D'Andrea, A.D. (2009). Inactivation of murine Usp1 results in genomic instability and a Fanconi anemia phenotype. Dev. Cell *16*, 314–320.

Kumari, U., Ya Jun, W., Huat Bay, B., and Lyakhovich, A. (2014). Evidence of mitochondrial dysfunction and impaired ROS detoxifying machinery in Fanconi anemia cells. Oncogene *33*, 165–172.

Lee, Y.S., Lee, J.W., Jang, J.W., Chi, X.Z., Kim, J.H., Li, Y.H., Kim, M.K., Kim, D.M., Choi, B.S., Kim, E.G., et al. (2013). Runx3 inactivation is a crucial early event in the development of lung adenocarcinoma. Cancer Cell *24*, 603–616.

Ley, T.J., Miller, C., Ding, L., Raphael, B.J., Mungall, A.J., Robertson, A.G., Hoadley, K., Triche, T.J., Laird, P.W., Baty, J.D., et al.; Cancer Genome Atlas Research Network (2013). Genomic and epigenomic landscapes of adult de novo acute myeloid leukemia. N. Engl. J. Med. *368*, 2059–2074.

Liu, P., Tarlé, S.A., Hajra, A., Claxton, D.F., Marlton, P., Freedman, M., Siciliano, M.J., and Collins, F.S. (1993). Fusion between transcription factor CBF beta/PEBP2 beta and a myosin heavy chain in acute myeloid leukemia. Science *261*, 1041–1044.

Maddipoti, S.C., Bueso-Ramos, C., Yang, H., Fernandez, M., Kuang, S., Fang, Z., Stevenson, W., Wei, Y., Pierce, S., and Garcia-Manero, G. (2008). Epigenetic silencing of the RUNX3 gene by promoter hypermethylation in patients with acute myeloid leukemia. Blood *112*, 3341–3341.

Mason, J.M., and Sekiguchi, J.M. (2011). Snm1B/Apollo functions in the Fanconi anemia pathway in response to DNA interstrand crosslinks. Hum. Mol. Genet. *20*, 2549–2559.

Meyers, S., Lenny, N., Sun, W., and Hiebert, S.W. (1996). AML-*2* is a potential target for transcriptional regulation by the t(8;21) and t(12;21) fusion proteins in acute leukemia. Oncogene *13*, 303–312.

Moldovan, G.L., and D'Andrea, A.D. (2009). How the fanconi anemia pathway guards the genome. Annu. Rev. Genet. *43*, 223–249.

Mosca, L., Musto, P., Todoerti, K., Barbieri, M., Agnelli, L., Fabris, S., Tuana, G., Lionetti, M., Bonaparte, E., Sirchia, S.M., et al. (2013). Genome-wide analysis of primary plasma cell leukemia identifies recurrent imbalances associated with changes in transcriptional profiles. Am. J. Hematol. *88*, 16–23.

Motoda, L., Osato, M., Yamashita, N., Jacob, B., Chen, L.Q., Yanagida, M., Ida, H., Wee, H.J., Sun, A.X., Taniuchi, I., et al. (2007). Runx1 protects hematopoietic stem/progenitor cells from oncogenic insult. Stem Cells *25*, 2976–2986.

Nakanishi, K., Yang, Y.G., Pierce, A.J., Taniguchi, T., Digweed, M., D'Andrea, A.D., Wang, Z.Q., and Jasin, M. (2005). Human Fanconi anemia monoubiquitination pathway promotes homologous DNA repair. Proc. Natl. Acad. Sci. USA *102*, 1110–1115.

Naoe, Y., Setoguchi, R., Akiyama, K., Muroi, S., Kuroda, M., Hatam, F., Littman, D.R., and Taniuchi, I. (2007). Repression of interleukin-4 in T helper type 1 cells by Runx/Cbf beta binding to the Il4 silencer. J. Exp. Med. *204*, 1749–1755.

Osato, M. (2004). Point mutations in the RUNX1/AML1 gene: another actor in RUNX leukemia. Oncogene *23*, 4284–4296.

Parmar, K., Kim, J., Sykes, S.M., Shimamura, A., Stuckert, P., Zhu, K., Hamilton, A., Deloach, M.K., Kutok, J.L., Akashi, K., et al. (2010). Hematopoietic stem cell defects in mice with deficiency of Fancd2 or Usp1. Stem Cells *28*, 1186–1195.

Pulliam-Leath, A.C., Ciccone, S.L., Nalepa, G., Li, X., Si, Y., Miravalle, L., Smith, D., Yuan, J., Li, J., Anur, P., et al. (2010). Genetic disruption of both Fancc and Fancg in mice recapitulates the hematopoietic manifestations of Fanconi anemia. Blood *116*, 2915–2920.

Speck, N.A., and Gilliland, D.G. (2002). Core-binding factors in haematopoiesis and leukaemia. Nat. Rev. Cancer *2*, 502–513.

Taniuchi, I., Osato, M., Egawa, T., Sunshine, M.J., Bae, S.C., Komori, T., Ito, Y., and Littman, D.R. (2002). Differential requirements for Runx proteins in CD4 repression and epigenetic silencing during T lymphocyte development. Cell *111*, 621–633.

Vandenberg, C.J., Gergely, F., Ong, C.Y., Pace, P., Mallery, D.L., Hiom, K., and Patel, K.J. (2003). BRCA1-independent ubiquitination of FANCD2. Mol. Cell *12*, 247–254.

Wang, H., Fan, R., Wang, X.Q., Wu, D.P., Lin, G.W., Xu, Y., and Li, W.Y. (2013a). Methylation of Wnt antagonist genes: a useful prognostic marker for myelodysplastic syndrome. Ann. Hematol. *92*, 199–209.

Wang, C.Q., Motoda, L., Satake, M., Ito, Y., Taniuchi, I., Tergaonkar, V., and Osato, M. (2013b). Runx3 deficiency results in myeloproliferative disorder in aged mice. Blood *122*, 562–566.

Yamamoto, K., Hirano, S., Ishiai, M., Morishima, K., Kitao, H., Namikoshi, K., Kimura, M., Matsushita, N., Arakawa, H., Buerstedde, J.M., et al. (2005). Fanconi anemia protein FANCD2 promotes immunoglobulin gene conversion and DNA repair through a mechanism related to homologous recombination. Mol. Cell. Biol. *25*, 34–43.

Yano, T., Ito, K., Fukamachi, H., Chi, X.Z., Wee, H.J., Inoue, K., Ida, H., Bouillet, P., Strasser, A., Bae, S.C., and Ito, Y. (2006). The RUNX3 tumor suppressor upregulates Bim in gastric epithelial cells undergoing transforming growth factor beta-induced apoptosis. Mol. Cell. Biol. *26*, 4474–4488.

Zaidi, S.K., Sullivan, A.J., van Wijnen, A.J., Stein, J.L., Stein, G.S., and Lian, J.B. (2002). Integration of Runx and Smad regulatory signals at transcriptionally active subnuclear sites. Proc. Natl. Acad. Sci. USA *99*, 8048–8053.